POLITECNICO DI TORINO
Repository ISTITUZIONALE

Finite fracture mechanics and cohesive crack model: Weight functions vs. cohesive laws

(Article begins on next page)

21 December 2022

FINITE FRACTURE MECHANICS AND COHESIVE CRACK MODEL: WEIGHT FUNCTIONS VS. COHESIVE LAWS

P. Cornetti[a,*], M. Muñoz-Reja[b], A. Sapora[a], A. Carpinteri[a]

[a] Department of Structural, Building and Geotechnical Engineering
Politecnico di Torino, Corso Duca degli Abruzzi 24, 10129, Torino, Italy.

[b] Grupo de Elasticidad y Resistencia de Materiales, Escuela Técnica Superior de Ingeniería,
Universidad de Sevilla, Camino de los Descubrimientos s/n, 41092 Sevilla, Spain

Abstract

The present work represents the prosecution of a previous paper [Short cracks and V-notches: Finite Fracture Mechanics vs. Cohesive Crack Model (2016). P. Cornetti, A. Sapora, A. Carpinteri. Engineering Fracture Mechanics 168:2-12] aiming to corroborate the use of Finite Fracture Mechanics by showing that its failure load estimates are very close to the ones provided by the well-established Cohesive Crack Model. While the above paper focused only on the Dugdale cohesive law and the original Finite Fracture Mechanics approach based on a point-wise stress condition, here we consider generic cohesive laws of power law type and propose an extension of Finite Fracture Mechanics based on stress weight functions. We argue that excellent agreement between the models is found provided proper correspondence rules between the shape of the cohesive laws and of the weight functions are given. As a test bench for this conjecture, we choose the Griffith crack geometry, where we are able to achieve the solutions in a semi-analytical way for both the models. Finally, we show that similar results can be obtained also by varying the domain of the weight function while keeping fixed its shape.

Keywords: Finite Fracture Mechanics, Cohesive Crack Model, Griffith Crack, Weight Functions.

1. Introduction

After the first pioneering papers by Barenblatt (1959), Dugdale (1960) and Hilleborg (1976), the Cohesive Crack Model (CCM) has been extensively used to analyze the fracture of plain or composite structures (e.g. Carpinteri, 1989; Needleman, 1990). The core of the CCM is represented by: (*i*) the cohesive law, a material property that describes macroscopically how the (cohesive)

(*) corresponding author. Email: pietro.cornetti@polito.it; tel.: +390110904901; fax: +390110904899

stresses decrease as the separation between crack faces increases up to complete detachment; (*ii*) the process zone, i.e. the length where cohesive stresses act.

One of the peculiarities of the CCM is its ability to predict crack initiation, a key-point where Linear Elastic Fracture Mechanics (LEFM) fails. This nice feature is shared with the more recent Finite Fracture Mechanics (FFM) model, resting on the assumption of a finite crack increment (in contrast with the infinitesimal growth assumed by LEFM). After the first pioneering paper by Hashin (1996), FFM received more and more attention following the fundamental work by Leguillon (2002), where the way to couple the stress condition for crack propagation with the discrete energy balance was set.

Implementation of the CCM requires a nonlinear finite element analysis with a very fine mesh, since an accurate resolution of the process zone (usually much smaller than the size of the structure) is needed. This is a drawback, since it means large computing times. On the other hand, FFM is much easier to apply since it just need a linear-elastic analysis. A good agreement between the two approaches is obviously welcome, since it means the possibility to replace CCM simulations with FFM analyses. Alternatively, wishing to retain the advantages of both the approaches, one can use FFM for preliminary sizing in structural design, letting the CCM for subsequent refinements, or, in numerical simulations of experimental tests, one can get through FFM a first estimate of the fracture parameters needed by the CCM.

For what concerns the comparison between FFM and CCM, preliminary results sound encouraging. Fair to excellent agreements were found for V-notched structures (Henninger et al., 2007; Murer & Leguillon, 2010; Cornetti et al., 2016), for open-holed plates (Rosendhal et al., 2017) for interfacial edge debonding in layered structures (Cornetti et al., 2015; Martin et al., 2016), for the pull-push test (Cornetti et al., 2012), for the double cantilever beam test (Dimitri et al., 2017), for the fiber-matrix debonding in composite materials (García et al., 2014; Távara et al., 2016) and for several adhesive lap joint geometries (Stein et al., 2015).

The agreement between CCM and FFM is not surprising since, despite the different – continuous vs. discrete – crack growth mechanism, the energy spent to create the new (unit) fracture surface is $\mathcal{G}_c$ for both the models (a condition usually not met by simple strength criteria and by the theory of critical distances, Taylor (2007)). Moreover, both CCM and FFM take the tensile strength into account: the CCM by means of the cohesive law shape, and the FFM by means of the expression of the stress condition. Up to now, an excellent correspondence has been found between the CCM with a constant cohesive law and the FFM approach with a point-wise stress requirement and between the CCM with a linearly descending cohesive law and the FFM approach with an average stress condition.

The aim of the present paper is twofold. On one hand, we provide an extension of the FFM approach by introducing a weight function into the stress condition. On the other hand, we investigate how to improve the matching between CCM and FFM failure load predictions by choosing suitable pairs of cohesive laws and the stress weight functions. The analysis is carried out mainly on a single geometry, i.e. the Griffith crack. Despite this could represent a limit of the present work, and further analyses are needed to verify the correspondence rules between cohesive laws and weight functions provided herein, the advantage of the chosen geometry is that CCM and FFM solutions are achieved in an analytical or semi-analytical form, allowing a deep insight on the problem at hand. However, at the end we present also the results for a couple of geometries with finite and vanishing sizes along with some comments.

The plan of the paper is as follows. In Section 2 we solve the Griffith crack according to the CCM, i.e. we derive the integral equation ruling the problem for an arbitrary cohesive law; furthermore, we provide a numerical technique to solve the equation and obtain the failure stress for softening laws of power law type. Then, in Section 3, we present a FFM extension based on the introduction into the stress condition of a weight function; we investigate the effect of its shape and domain. In Section 4, correspondence rules between weight functions and cohesive laws are proposed and checked for the considered geometry. Finally, we provide some conclusions in Section 5.

2. A Cohesive Crack Model solution for the Griffith Crack

As stated in the Introduction, we use as a test bench an infinite slab with a central crack of length $2a$ under a remote uni-axial stress σ_∞ orthogonal to the crack (i.e. the Griffith crack geometry, see Fig.1a). In this section, we provide a way to solve the problem according to the CCM, i.e. when the material obeys an arbitrary cohesive law inside the process zone, while remaining linear elastic outside. Note that Xu & Waas (2017) recently gave a solution to such a structural problem. However, for the sake of comparison with the FFM approach and because we used a different numerical technique (see below), in the present section we provide the details of the CCM solution.

2.1 Governing equation

In order to achieve the solution, one need two fundamental results by Linear Elastic Fracture Mechanics (LEFM). The former one is represented by the Stress Intensity Factor (SIF) K_I and the

Crack Opening Displacement (COD) *w* for the Griffith Crack, which are equal to, respectively (Fig.1a):

$$K_{\mathrm{I}} = \sigma_{\infty} \sqrt{\pi a} \tag{1}$$

$$w(x) = \frac{4\sigma_{\infty}}{E'} \sqrt{a^2 - x^2} \tag{2}$$

x being is the spatial coordinate as in Fig.1 and *E′* the Young modulus in plain strain conditions. The latter result consist of the SIF and the COD for a pair of opposite forces *P* acting on the crack faces at a distance *t* from the crack mid-point ($-a < t < +a$), see Fig.1b:

$$\left(K_{\mathrm{I}}\right)_{\pm a} = \frac{P}{\sqrt{\pi a}} \frac{\sqrt{a^2 - t^2}}{a \mp t} \tag{3}$$

$$w(x) = \frac{4P}{\pi E'} \mathrm{Arccosh} \frac{a^2 - t\, x}{a\, |x - t|} \tag{4}$$

Note that Eq.(3) provides both the crack tip SIFs: the first sign refers to the right crack tip ($x = +a$), the second one to the left crack tip ($x = -a$). For what concerns Eq.(4), it is worth noting that it is singular in $x = t$, i.e. where the force is applied, as reasonably expected in the linear elasticity framework. Finally, observe that both displacement functions in Eqs.(2) and (4) can be obtained starting from the SIF expressions given by Eqs.(1) and (3) according to Paris' equation (Tada et al., 2000), but their derivation is here omitted for the sake of brevity.

As well known, the CCM prescribes non-singular stress fields. Hence, for any tensile load, a process zone (of length a_{p}) appears ahead the crack tip where cohesive stresses σ_{coh} act in order to vanish the SIF at the so-called fictitious crack tip (Hillerborg, 1976), see Fig.2a. Thus, by the principle of effect superposition, we have that:

$$K_{\mathrm{I}}\left(\sigma_{\infty}\right) + K_{\mathrm{I}}\left(\sigma_{\mathrm{coh}}\right) = 0 \tag{5}$$

Provided that *a* is now replaced by ($a+a_{\mathrm{p}}$), the two terms at the left hand side are given by Eq.(1) and by integrating Eq.(3) over the process zone, respectively. Thus, Eq.(5) yields a relationship among the remote stress, the cohesive stresses and the process zone length, which, after some analytical manipulations, can be cast into:

4

$$\sigma_\infty = \frac{2}{\pi} \int_a^{a+a_p} \frac{\sigma_{coh}(t)}{\sqrt{(a+a_p)^2 - t^2}} \, dt \qquad (6)$$

Analogously to what done for the SIF, we can evaluate the COD by summing the contribution of the external load (Eq.(2)) and of the cohesive stresses (integrating Eq.(4)). By further substituting the remote stress with the expression given by Eq.(6), we finally get:

$$w(x) = \frac{4}{\pi E'} \int_a^{a+a_p} \sigma_{coh}(t) \left\{ 2\sqrt{\frac{(a+a_p)^2 - x^2}{(a+a_p)^2 - t^2}} - \left[\text{Arccosh} \frac{(a+a_p)^2 + t\,x}{(a+a_p)(x+t)} + \text{Arccosh} \frac{(a+a_p)^2 - t\,x}{(a+a_p)|x-t|} \right] \right\} dt$$

(7)

The CCM states that the cohesive stresses σ_{coh} in the process zone depend on the crack opening w according to a function named cohesive law (see Fig.2b); this function is hereafter marked as f in dimensionless form, i.e. $\tilde{\sigma}_{coh} = f(\tilde{w})$, being:

$$\tilde{\sigma}_{coh} = \frac{\sigma_{coh}}{\sigma_c}, \quad \tilde{w} = \frac{w}{w_c} \qquad (8)$$

the dimensionless cohesive stresses and opening displacements, respectively. The cohesive law describes how the cohesive stresses decrease from the material tensile strength σ_c to zero as the crack opening increases from 0 to its critical value w_c, i.e. the value at which the interactions between crack faces vanish. The area below the curve represents the fracture energy G_{Ic}, i.e. the energy necessary to create the unit fracture surface. The shape of the cohesive law as well as its parameters σ_c, w_c, G_{Ic} are assumed to be material properties. For the sake of simplicity, it is convenient to introduce also the parameter q, defined as the number whose inverse is the area below the dimensionless cohesive law:

$$\int_0^1 f(t) \, dt = \frac{1}{q} \qquad (9)$$

or, equivalently, $q = (\sigma_c \, w_c) \, / \, G_{Ic}$. Obviously, q is larger than or equal to 1.

Because of the cohesive law, it is clear that Eq.(7) is an integral equation in the displacement function. We can give it a dimensionless formulation by normalizing the process zone a_p, the horizontal coordinate x and the dummy variable t with respect to the crack length a, i.e.:

$$\beta = \frac{a + a_p}{a} \quad , \quad \xi = \frac{x}{a} \quad , \quad \tau = \frac{t}{a} \tag{10}$$

The following inequalities hold: $\beta > 1$, $1 < \xi < \beta$ and $1 < \tau < \beta$. The crack length a is then conveniently normalized with respect to Irwin's characteristic length l_{ch}:

$$\alpha = \frac{a}{l_{ch}} \quad , \quad l_{ch} = \frac{\mathcal{G}_{Ic} E'}{\sigma_c^2} \tag{11}$$

Introducing the (weakly singular) kernel function g as:

$$g(\beta, \xi, \tau) = 2\sqrt{\frac{\beta^2 - \xi^2}{\beta^2 - \tau^2}} - \left[\operatorname{Arccosh} \frac{\beta^2 + \tau\xi}{\beta(\xi + \tau)} + \operatorname{Arccosh} \frac{\beta^2 - \tau\xi}{\beta|\xi - \tau|} \right] \tag{12}$$

by some analytical manipulations, Eq.(7) becomes:

$$\tilde{w}(\xi) = \frac{4\alpha}{\pi q} \int_1^\beta f\left[\tilde{w}(\tau)\right] g(\beta, \xi, \tau)\, d\tau \tag{13}$$

In this form, it is apparent that, from a mathematical point of view, the problem at hand reduces to the solution of a weakly singular nonlinear Fredholm integral equation of the second kind. One can also choose as unknown variable the cohesive stresses instead of the opening displacement; in this second way, we get:

$$f^{-1}\left[\tilde{\sigma}_{coh}(\xi)\right] = \frac{4\alpha}{\pi q} \int_1^\beta \tilde{\sigma}_{coh}(\tau)\, g(\beta, \xi, \tau)\, d\tau \tag{14}$$

where f^{-1} represents the inverse of the cohesive law f. Once f is defined (and hence q by Eq.(9)), the solution of either Eq.(13) or (14) depends only on the two parameters α and β, i.e. on the crack and

process zone length. The corresponding remote stress is then determined by means of Eq.(6), which, in dimensionless form, reads:

$$\frac{\sigma_\infty}{\sigma_c} = \frac{2}{\pi} \int_1^\beta \frac{\tilde{\sigma}_{coh}(\tau)}{\sqrt{\beta^2 - \tau^2}} d\tau \qquad (15)$$

Wishing to determine the failure stress σ_f, one has to fix α and then let β slowly increase starting from zero. The remote stress is firstly increasing and then decreasing: its maximum value represents the failure stress σ_f. Note that the maximum is always achieved before the opening displacement reaches its critical value w_c at $x = a$ (i.e. when the real crack tip starts moving), except for the Dugdale cohesive law. Moreover, in order to obtain the failure stress vs. the crack length diagram, the procedure has to be repeated for different α values.

Eq.(13) can be solved analytically only for a Dugdale cohesive law, i.e. for constant cohesive stresses. Accordingly, $f \equiv 1$ and Eq.(13) reverts to the evaluation of an integral (see e.g. Broberg, 1999; Cornetti et al., 2016). In all the other cases, the equation has to be solved numerically; in the next subsection, we provide a way to do it.

2.2 Numerical solution

For numerical reasons, it is easier to solve Eq.(14) instead of Eq.(13). To this aim, we follow a procedure somewhat similar to the one proposed by Lenci (2001) to obtain the stress field for a (Griffith) crack at a weak interface. The basic idea is to express the unknown function in series and then to determine the coefficients of the series by minimizing the difference between the two sides of Eq.(14).

In the present case, we approximate the cohesive stress function in power series, i.e. as a polynomial of order k:

$$\tilde{\sigma}_{coh}(\xi) = \sum_{i=0}^{k} c_i \xi^i = c_0 + c_1\xi + c_2\xi^2 + \ldots + c_k\xi^k \qquad (16)$$

The problem unknowns are now the coefficients c_i ($i = 1,\ldots, k$) of the polynomial. The first coefficient c_0 is excluded since it can be expressed as a function of the other coefficients: in fact, at the fictitious crack tip, the stress equals the tensile strength, i.e. $\tilde{\sigma}_{coh}(\beta) = 1$. Thus:

$$c_0 = -\sum_{i=1}^{k} c_i \beta^i \qquad\qquad (17)$$

Let us now define m equally spaced points within the interval $1 \le \xi \le \beta$. Their abscissa ξ_j is:

$$\xi_j = 1 + \frac{j-1}{m-1}(\beta-1), \qquad j = 1,\ldots,m \qquad\qquad (18)$$

The coefficients c_i of the polynomial (16) are then determined by minimizing the Mean Square Error between the two sides of Eq.(14) evaluated at $\xi = \xi_j$ ($j = 1,\ldots, m$). In formulae:

$$\min_{c_1,c_2,\ldots,c_k} \left\{ \frac{1}{m} \sum_{j=1}^{m} \left[f^{-1}\left(\sum_{i=0}^{k} c_i \xi_j^i \right) - \frac{4\alpha}{\pi q} \sum_{i=0}^{k} c_i h_i(\beta,\xi_j) \right]^2 \right\} \qquad (19)$$

where:

$$h_i(\beta,\xi) = \int_{1}^{\beta} \tau^i\, g(\beta,\xi,\tau)\, \mathrm{d}\tau \qquad\qquad (20)$$

Although the kernel function g (given by Eq.(12)) is twice singular (at $\tau = \xi$ and $\tau = \beta$, respectively), the integrals in Eq.(20) can be evaluated in a closed form; thus, there is no loss of precision due to the singularities. More precisely, h_0, h_1 are easily achieved; then, through integration by parts and suitable analytical manipulations, we get a recursive formula providing h_i as a function of h_{i-2}; functions h_0, h_1 and the recursive formula are reported in the appendix.

A further advantage of the proposed numerical procedure is that the value of the minimum provides an information about the accuracy of the solution. The root of Eq.(19) represents the Root of the Mean Square Error (RMSE) and, obviously, the lower it is, the more precise the solution. In all the subsequent calculations, we assume $k = 8$ and $m = 50$, values that we considered satisfactory since they always provided a RMSE within the range $10^{-5} \div 10^{-3}$; moreover higher k and m values did not provide a significant reduction of the RMSE.

As an example we show, for a given crack length and for the case of linear softening (i.e. $\tilde{\sigma}_{coh} = 1 - \tilde{w}$), how to compute the stress and displacement fields within the process zone, as well as

the failure stress. Note that, in this particular case, it is also possible to obtain the solution assuming that the unknown function is piecewise linear and Eq.(13) reverts to the solution of a linear system. However, the method proposed here is more general, being applicable also to non-linear softening laws, as done in the following. For the linear softening case, $q = 2$ and the expression to be minimized (Eq.(19)) becomes:

$$\min_{c_1,c_2,...c_k} \left\{ \frac{1}{m} \sum_{j=1}^{m} \left[\left(1 - \sum_{i=0}^{k} c_i \xi_j^i \right) - \frac{2\alpha}{\pi} \sum_{i=0}^{k} c_i h_i (\beta, \xi_j) \right]^2 \right\} \tag{21}$$

We set, for instance, $\alpha = 1$ (i.e. $a = l_{ch}$). Then we solve the minimization problem (21) for increasing β values (starting from 1): at each step the coefficients c_i define the stress and displacement fields. As β increases, the remote stress (given by Eq.(15)) increases. The maximum is reached at $\beta = 1.691$ (i.e. for a process zone length $a_p = 0.691\ a$) when the remote (failure) stress is $\sigma_\infty = \sigma_f = 0.478\ \sigma_c$; the corresponding RMSE is $7.6\ 10^{-5}$. The load then decreases up to $\beta = 1.899$, when the opening displacement reaches its critical value and the cohesive stresses vanish at $x = a$ (i.e. $\tilde{w}(1)=1$, $\tilde{\sigma}_{coh}(1) = 0$ and the real crack starts growing). For such a β value (i.e. for a process zone length $a_p = 0.899\ a$), we obtain $\sigma_\infty = 0.461\ \sigma_c$ and a RMSE equal to $6.9\ 10^{-5}$. For these two cases, displacement and stress fields within the process zone are plotted in Figs.3a and 3b, respectively.

As mentioned above, it is worth observing that the same structural problem has been very recently considered by Xu & Waas (2017). They derived the integral equation Eq. (14) and provided a numerical solution for the linear softening case. Their numerical approach is completely different from the one we followed. The main differences are: (*i*) the continuous stress distributed within the cohesive zone is modeled by a number of discrete uniform segment stress, whereas in the present manuscript is approximated by a polynomial function valid on the whole cohesive zone; (*ii*) the control parameter is the remote stress and the process zone is the outcome (herein is the opposite, the process zone length being the input and the remote stress the output). Consequently, Xu & Waas (2017) detected multiple solutions, in the sense that, close to the peak value of the remote stress, they found two different admissible values for the process zone size. See also Xu et al. (2014).

2.3 Failure stress vs. crack length according to power cohesive laws

Following the procedure previously outlined, i.e. fixing α and letting β to increase until the remote stress reaches the maximum, we determine the failure stress vs. crack length for different cohesive laws. More in detail, we consider power cohesive laws, that is:

$$\tilde{\sigma}_{coh} = \left(1 - \tilde{w}\ \right)^n \tag{22}$$

where n is a positive number. In Fig.4a the cohesive law (22) is plotted for the following values: $n = 0$ (Dugdale cohesive law), $n = 1/2$ (corresponding to a concave cohesive law), $n = 1$ (linear softening), $n = 2$ and $n = 4$ (corresponding to convex cohesive laws); see also Table 1, third column. Wishing to isolate the effect of the shape of the cohesive law, the comparison is performed keeping the fracture energy and the tensile strength constant, so that the cohesive laws actually compared are the ones drawn in Fig.4b. The parameter q is equal to $n + 1$ and represents the abscissa of the point at which the cohesive stress vanishes according to the different cohesive laws.

In Fig.5a we plot the normalized failure stress vs. the normalized crack length according to the CCMs and, for the sake of comparison, to the LEFM (i.e. $\sigma_f/\sigma_c = 1/\sqrt{\pi\alpha}$). It is evident that the higher n (i.e. the steepest the cohesive stress decrement), the lower the failure stress is. Moreover, the effect of the parameter n decreases as n itself increases. In the Scientific Literature (see e.g. Shet & Chandra, 2004; Alfano, 2006; Wang, 2013) there are several papers highlighting the effect of the shape of the cohesive law, usually concluding that it is rather small (at fixed $\mathcal{G}_c$ and σ_c). We agree that the effect is small (it is null for $\alpha = 0$ and $\alpha \to \infty$); however, it is not always negligible, as it reaches the 30% between the predictions of the extreme cases herein considered ($n = 0$ and $n = 4$ respectively) for α values close to $1/\pi$ (when the LEFM prediction crosses the tensile strength). As expected, all the CCM curves tend asymptotically to the LEFM curve for large cracks (i.e. for large sizes). Finally, in Fig.5b we plotted the normalized process zone size vs. the crack length at failure stress. It is worth noting the different trend: monotonically decreasing for small n ($n = 0, 0.5$) and monotonically increasing for large n ($n = 1, 2, 4$).

3. Weight functions for Finite Fracture Mechanics

Finite Fracture Mechanics is a fracture criterion resting on the assumption of a finite crack advancement, i.e. the infinitesimal energy balance by Griffith is replaced by a discrete energy balance: crack grows by a finite step Δ if the energy available is equal or larger than $\mathcal{G}_{Ic} \times \Delta$. For

mode I problems in homogeneous materials and recalling Irwin's relationship $G = K_\mathrm{I}^2/E'$, this condition can be written as:

$$\int\limits_{a}^{a+\Delta} K_\mathrm{I}^2(a')\,\mathrm{d}a' \ge K_\mathrm{Ic}^2 \Delta \tag{23}$$

where the crack length a may be zero if the original geometry is un-cracked. This a necessary condition for crack to grow. It becomes also a sufficient condition if, at the same time, the (average) stress exceeds the material tensile strength on the length Δ where crack will grow:

$$\sigma_\mathrm{y}(x) \ge \sigma_\mathrm{c} \text{ for } a < x < a+\Delta \qquad \text{or} \qquad \int\limits_{a}^{a+\Delta} \sigma_\mathrm{y}(x)\,\mathrm{d}x \ge \sigma_\mathrm{c}\,\Delta \tag{24}$$

For usual cases (positive geometries), the $K_\mathrm{I}(a)$ and $\sigma_\mathrm{y}(x)$ functions are monotonically increasing and decreasing respectively. In such a case, the minimum (actual) failure load is the one for which the two inequalities (23) and (24) are strictly fulfilled; correspondingly, FFM reverts to the solutions of two equations in two unknowns, the finite crack advance Δ and the failure load, implicitly embedded in $K_\mathrm{I}(a)$ and $\sigma_\mathrm{y}(x)$.

Before proceeding, it is worth observing that the energy available for the finite crack growth is conveniently obtained by integrating (the square of) the SIF (left hand side of Eq. (23)) as far as the SIF function is known analytically (like for the Griffith crack case herein considered) or approximated expressions are available from Fracture Mechanics Handbooks (Tada et al, 2000). If this is not case, it is preferable its evaluation by suitable path-independent integrals exploiting the linear elastic solution before and after the finite crack advance (see e.g. Leguillon (2002), where semi-analytical results are obtained by the asymptotic matching technique) or by evaluating numerically the crack closure work either by Finite or Boundary Element Analyses (see e.g. Becker et al. 2010; Sun et al. 2015).

Up to now, in mode I problems, the discrete energy balance has been coupled with a point-wise (Leguillon, 2002) or to an average (Cornetti et al., 2006) stress requirement – see eqn (24). In order to get FFM more flexible, in the following we propose a generalized stress condition based on the introduction of weight functions. The basic idea is that materials show different microstructural features when cracking; these different behaviors can be phenomenologically taken into account by weighting differently the stresses ahead the crack tip, similarly to what occurs for the CCM, where different cohesive law shapes refer to different materials / micro-cracking mechanisms.

Before starting, it is worth noting that weight functions can be applied to the strain energy release rate (during the finite crack growth) as well: see, for instance, Bažant (2001) or the so-called Equivalent-LEFM criterion, according to which the strain energy release rate (or the SIF) is evaluated for an equivalent crack larger than the real one. However, such a procedure implies a violation of the energy balance, i.e. the energy released during the finite crack growth does not coincide with the energy necessary to create the new crack surface. Thus, we decide to preserve the discrete energy balance as in the original FFM formulation (also for the sake of comparison with the CCM, which satisfies the energy balance as well) and to act only onto the stress condition.

Hence, let us introduce the weight function $\rho(t)$, which, by definition, fulfills the condition:

$$\int_{-\infty}^{+\infty} \rho(t)\, dt = 1 \tag{25}$$

According to the (generalized) FFM, a crack of length a placed along the x-axis and loaded in mode I will propagate if the two following conditions are fulfilled:

$$\begin{cases} \int_a^\infty \sigma_y(x)\, \rho\left(\dfrac{x-a}{\Delta}\right) dx \geq \sigma_c\, \Delta \\[2mm] \int_a^{a+\Delta} K_I^2(a')\, da' \geq K_{Ic}^2 \Delta \end{cases} \tag{26}$$

System (26) holds true also for initially un-cracked specimens (e.g. notched specimens), when a is null. For usual cases, as the present one (i.e. positive geometries), the stress field is monotonically decreasing along x and the SIF is monotonically increasing along with a; thus, the minimum failure load satisfying the system (26) is the one for which the two inequalities are strictly satisfied.

Westergaard's solution provides the stress field for the Griffith crack geometry. Ahead the crack tip ($x > a$), it reads:

$$\sigma_y(x) = \frac{x}{\sqrt{x^2 - a^2}}\, \sigma_\infty \tag{27}$$

At incipient failure, substitution of Eqs. (1) and (27) into system (26) yields (in dimensionless form):

$$\begin{cases} \dfrac{\sigma_f}{\sigma_c} \displaystyle\int_\alpha^\infty \dfrac{\tilde{\xi}}{\sqrt{\tilde{\xi}^2 - \alpha^2}}\ \rho\!\left(\dfrac{\tilde{\xi}-\alpha}{\tilde{\delta}}\right) d\tilde{\xi} = \tilde{\delta} \\[4mm] \dfrac{\sigma_f}{\sigma_c} = \sqrt{\dfrac{2}{\pi\,(2\alpha + \tilde{\delta})}} \end{cases} \tag{28}$$

where now all the lengths have been normalized with respect to the internal length, i.e. $\tilde{\xi} = x/l_{ch}$ and $\tilde{\delta} = \Delta/l_{ch}$. Eq.(28) represents a system of two equations in two unknowns, i.e. the failure remote stress (σ_f/σ_c) and the finite crack increment $\tilde{\delta}$, whose solution depends on the normalized crack length α and the choice of the weight function ρ. Wishing to investigate the effect of ρ, we will first fix the domain of the weight function and let vary its shape; then, we will fix the shape and let the domain/position vary.

3.1 Effect of the shape of the weight function

In this former case, we assume that the (and only the) stresses acting where the crack grows by a finite amount affect crack propagation, i.e. the weight function $\rho(t)$ differs from zero for $0 < t < 1$. In Fig.6a we plot the following weight functions, all equal to zero outside of the interval [0,1]:

$$\rho(t) = 3(1-t)^2 \tag{29a}$$

$$\rho(t) = 1 \tag{29b}$$

$$\rho(t) = 6\,t\,(1-t) \tag{29c}$$

$$\rho(t) = 3t^2 \tag{29d}$$

$$\rho(t) = \delta(1-t) \tag{29e}$$

where $\delta(\cdot)$ denotes the Dirac delta function. Before proceeding, it is worth noting that the second and the fifth cases correspond to the FFM versions currently used. The choice of a uniform weight function in Eq.(26) is tantamount to assume that fracture propagates when the average stress reaches the tensile strength. The corresponding solution for the Griffith crack was provided in Cornetti et al. (2006): the finite crack step does not depend on the crack length, being always equal to $(2/\pi)\times l_{ch}$. On the other hand, the Dirac delta weight function (Eq.(29e)) corresponds to a point-

wise stress requirement. Recalling the scaling property $\delta(c\,t) = \delta(t)/|c|$ (c constant), it is evident that in such a case Eq.(26) reverts to the FFM criterion proposed by Leguillon (2002) (for monotonically decreasing stresses), i.e. fracture propagates if the stress all over the finite crack increment is larger than the tensile strength. The corresponding solution for the Griffith crack, yielding a cubic equation in the finite crack step, can be found in Cornetti et al. (2016). In all the other cases, the integral in the stress condition is achieved analytically but the final equation in the crack increment has to be solved numerically.

The failure remote stresses and the finite crack advancements, i.e. the solutions of system (28), are given in Fig.6b and 6c respectively, according to the different weight functions provided by Eqs.(29). Depending on the choice of the weight function, the trend of crack increment can be either increasing, constant or decreasing with the crack length (see Fig.6c). Obviously, the failure remote stress is always monotonically decreasing (Fig.6b): all the curves start from the tensile strength and tend to LEFM for large cracks. This aspect is particularly evident in the bi-logarithmic plot of Fig.6d, where one clearly sees that plots related to different weight functions share the same small and large size asymptotes. On the other hand, it is clear that failure stress predictions vary in between, and that weight functions higher in the neighborhood of the origin (i.e. closer to the crack tip) provide lower failure stress predictions.

3.2 Effect of the domain/position of the weight function

In this latter case, we fix the weight function shape but let its domain or its position vary. As an example, we can take a uniform weight function whose domain is more or less large according to the value of the parameter p:

$$\rho(t) = \begin{cases} p, & 0 < t < \dfrac{1}{p} \\ 0 & \text{elsewhere} \end{cases} \tag{30}$$

The higher is p, the smaller the domain where stress is averaged, the lower the failure stress expected. For instance, $p = 2$ means averaging the stress over a length equal to half the finite crack step.

A second possibility is to choose the Dirac delta function as the weight function, but placed in different points according to the p value:

$$\rho(t) = \delta(1 - p\,t) \tag{31}$$

$p = 1$ corresponds to Leguillon's FFM version (for monotonically decreasing stresses), when the stress is required to exceed the tensile strength all over the crack increment Δ. On the other hand, taking $p > 1$ means that fracture propagates by a finite step Δ if the discrete energy balance is fulfilled and the stress is larger than the tensile strength over a fraction $1/p$ of the crack increment Δ. Of course, the higher is p, the easier is satisfying the stress requirement and the lower the expected failure stress. Conversely, taking $p < 1$ means that the discrete energy balance needs to be fulfilled for crack increments Δ equal to a fraction p of the length where the stresses exceed the tensile strength, thus leading to higher failure stress predictions.

These expected behaviors are easily checked by substituting Eq.(31) into system (28), whose solution yields the following cubic equation in the dimensionless crack increment:

$$2(\alpha + \tilde{\delta}/p)^2 = \pi(2\alpha + \tilde{\delta})(2\alpha + \tilde{\delta}/p)\tilde{\delta}/p \tag{32}$$

which generalizes the one provided in Cornetti et al. (2016) for $p = 1$. The corresponding failure stresses are then obtained, e.g., by the second equation in system (28). The solutions are plotted in Fig.7 in terms of failure stress (Fig.7a) and finite crack increment (Fig.7b) vs. crack length; in this latter case, as in the previous subsection, the trend can be either increasing, (approximately) constant or decreasing depending on the weight function (i.e., in the present case, on the parameter p). It is evident that increasing p the failure stress decreases and the finite crack step increases. Noteworthy, as $p \to 0$, the failure stress tends to the minimum between the tensile strength σ_c and the LEFM prediction $\sigma_f = K_{Ic}/\sqrt{\pi a}$; correspondingly, the finite crack increment tends to vanish for $a > l_{ch}/\pi$, i.e. the discrete energy balance becomes infinitesimal.

Finally, for what concerns the finite crack step, it is worth noting that it tends to the constant value $2/\pi \times l_{ch}$ when the crack vanishes independently of the p value. Conversely, for very large cracks, the finite crack increment Δ tends to the asymptotic value $p \times l_{ch}/(2\pi)$, i.e. the region where the stress exceeds the tensile strength (i.e. Δ/p) tends to the constant value $l_{ch}/(2\pi)$ independently from p, as highlighted in Fig.7c.

4. Correspondence rules between weight functions and cohesive laws

Although based on different assumptions, CCM and FFM usually provide very similar results because they are based on the same material parameters (fracture energy and tensile strength) and they both require the same amount of (surface) dissipated energy. To the authors' best knowledge, significant discrepancies may occur, especially for the point-wise FFM version, only for very small structures (i.e. in the small-scale asymptote in a size effect analysis) when the crack step / process zone tend to cover the whole ligament (Cornetti et al., 2006). Indeed, this represents a case of little practical interest and still controversial from a theoretical point of view (for a review on the subject see e.g. Carpinteri et al., 2006). On the other hand, as evident also from the analysis carried out in the present paper, the CCM solution is much more troublesome to be achieved with respect to the FFM one. Thus, FFM can be seen either as an effective alternative approach to CCM or as a suitable tool for preliminary sizing, restricting the use of the computationally demanding CCM to the last stage of the structural project.

Aim of the present section is to provide some empirical rules matching CCM and FFM solutions in the best way. According to what presented in the previous section, this can be achieved either by properly shaping the weight function or by varying its domain/position.

Up to now, an excellent agreement has been observed between these two pairs: CCM with a Dugdale cohesive law and FFM with a point-wise stress criterion (Henninger et al., 2007; Cornetti et al., 2016); CCM with a linear softening and FFM with an average stress condition (Cornetti et al., 2012; Rosendahl et al., 2017). Starting from this observation, we may formulate the following conjecture: CCM and FFM predictions match (approximately) each other if the weight function is the derivative of the cohesive law with opposite sign. In formulae:

$$\rho(t) = \begin{cases} -f'(t), & 0 \le t \le 1 \\ 0 & \text{elsewhere} \end{cases} \tag{33}$$

Eq.(33) implies giving a heavier weight to the stresses located where the cohesive law is steeper. Actually, Dugdale cohesive law presents a sudden stress drop and (the opposite of) its derivative (in dimensionless terms) is the Dirac delta function, whereas the derivative of the linear softening cohesive law is the unit function; thus the matching already observed in the Scientific Literature is respected by Eq.(33). Wishing to see if it works also for other pairs, we solved the FFM system (28) for weight functions given by Eqs. (22) and (33), i.e.:

$$\rho(t) = n(1-t)^{n-1} \tag{34}$$

and compared the FFM solutions with the CCM solutions obtained in Section 2 (that is, for $n = 0$, 0.5, 1, 2, 4). The corresponding pairs are given in Table 1 (columns 2 and 3), the cohesive laws being plotted in Fig.4a and the weight functions in Fig.8a. The FFM and CCM failure stress solutions are drawn in Fig.8b. It is evident the good agreement (almost perfect for $n = 2$), the difference between corresponding pairs being always smaller 6 %. Finally, in Fig.8c the finite crack increment is plotted vs. the crack length. Although the FFM crack increments and the CCM process zone are definitely different quantities (as expected, since they possess different physical meanings), the comparison between Fig.5b and Fig.8c clearly shows that they share the same trend: monotonically decreasing for n equal to 0 and 0.5, approximatively constant for $n = 1$ and increasing for n equal to 2 and 4.

The matching between CCM and FFM can be improved also by varying the parameter p in the FFM approach provided in Section 3.2. In this case, we simply looked for the p value providing the better agreement with the CCM solutions given in Section 2 for different n values: results are presented in Table 1 (columns 3 and 4). The comparison between the CCM and FFM failure stresses are given in Fig.9a, whereas the FFM crack increments are provided in Fig.9b. It is remarkable the excellent agreement between the curves in Fig.9a (differences between corresponding pairs always below 4%, and significant only for very small crack lengths) as well as the similar trends shown by the FFM crack increments in Fig.9b and the CCM process zones in Fig.5b.

Interpolating the discrete results of Table 1, we propose the following correspondence rule between the parameters p and n:

$$p = 1.5 + 5.5\,n - 1.06\,n^2 + 0.070\,n^3 \tag{35}$$

The interpolation function (35) is plotted in Fig.10. It is interesting to observe that for the Dugdale CCM ($n = 0$), the best agreement is obtained if we require that the stress exceeds the tensile strength not over the whole crack step Δ (as in Leguillon's version) but only over about 2/3 Δ ($p \cong 1.5$). Furthermore, for softening cohesive laws, the fraction of the crack increment where stress must exceed the tensile strength can be really small (e.g. $\sim\Delta/9$ for a parabolic softening, i.e. $n = 2$).

Before concluding, it is worth observing that the proposed correspondence rules have been checked only for the Griffith crack geometry; further investigations are needed to check if they work also for other (finite) geometries. Nevertheless, our feeling is that relationships given by Eqs.(33) and (35) have a broader validity, at least for mode I problems in homogeneous linear elastic isotropic materials. In fact, both CCM and FFM are able to catch the effect of

boundaries/finite size since both the process zone and the finite crack advancement are structural (and not merely material) parameters. As a preliminary result, here we simply provide a couple of examples for finite size geometries. The former one refers to Three Point Bending cracked specimens: the relative crack depth varies between 0.05 and 0.5 (see fig. 11a), while specimen height is about four times Irwin's length (relatively small specimens). CCM data are taken from Carpinteri & Colombo (1989) and are related to a linear softening cohesive law. The FFM predictions were obtained (by exploiting the SIF given in Tada et al. (2000) and the stress field provided in Karihaloo & Xiao (2001)) by means of the proposed correspondence rules, i.e. with a constant weight function and with p equal to 6. It is evident the excellent agreement, while LEFM provides significantly higher nominal failure stresses. The latter example refers to Three Point Bending plain specimens, highlighting the size effect on the flexural strength (fig. 11b). As above, CCM data are taken from Carpinteri & Colombo (1989) and relate to a linear softening cohesive law, while we used simple beam theory for the stress field to be used in the FFM approach. Since there is no crack, LEFM is not able to predict any failure; on the other hand, theory of critical distances (requiring that the average stress over the material length $\Delta = [(2/\pi) \times l_{ch}]$ exceeds the tensile strength σ_c) provide an unrealistic infinite strength as the specimen height tends to Δ. On the other hand and noteworthy, the trend provided by FFM and CCM is still similar for sizes lower than l_{ch}, although the asymptotic limit for vanishing size is the same only if one takes $p = 3$ in the FFM approach.

Extracting the cohesive law parameters from experimental data is not an easy task (see e.g. Xu et al. 2015); the same occurs with the extended FFM model we propose. Which are the best experiments to determine the extended FFM parameters is a problem we will not address in the present paper. Here, we simply observe that, being the FFM approach easier to apply with respect to the CCM, also getting an estimate of the FFM parameters from experimental data fitting is relatively less complicated. Moreover, by means of the correspondence between CCM and FFM given in the present manuscript, one can gather also some indirect information about the cohesive law shape and parameters. In this sense, FFM has been already used by Martin et al. (2016) to get a first estimate of the linear softening cohesive crack model parameters (for the description of edge debonding in a bimaterial specimen).

5. Conclusions

In the present paper, we have tried to highlight similarities, differences and correspondences between the FFM approach and the CCM. Although only one, ideal, geometry is considered, we

have provided the solution according the two models in an almost analytical fashion, thus allowing a deep insight to the comparison.

With respect to previous work available in the Scientific Literature, the main novelty here is a generalization of the FFM approach obtained by introducing a weight function into the stress condition. Then, weight functions are used to achieve a good match with the CCM predictions: a nice agreement is found if suitable pairs of cohesive laws and weight functions are chosen. More in details, CCMs showing cohesive laws with earlier softening usually match satisfactorily with FFM stress conditions characterized by weight functions higher close to the crack tip and vice-versa. The reason for this is that a quick decay of the cohesive stresses (at constant fracture energy, meaning the presence of long tails) implies a large process zone, with relatively low stresses and, finally, a relatively low failure load according to the CCM approach. Analogously, a higher weight for the stresses close to the tip means a larger lower bound for the admissible crack increment according to the stress condition. This implies larger finite crack steps with lower stresses and, finally, lower failure loads according to the FFM criterion.

Summarizing, the results shown in the present paper prove once more the soundness of the Finite Fracture Mechanics approach, alone or coupled with the CCM. In this latter case, FFM can be useful for preliminary sizing in structural design, letting the CCM to refinements, or for providing a first estimate of the CCM parameters when interpreting experimental tests.

6. Appendix

Functions h_0 and h_1 are given by:

$$h_0(\beta,\xi) = \int_1^\beta g(\beta,\xi,\tau)\,\mathrm{d}\tau = (\xi+1)\,\mathrm{Arccosh}\,\frac{\beta^2+\xi}{\beta(\xi+1)} - (\xi-1)\,\mathrm{Arccosh}\,\frac{\beta^2-\xi}{\beta(\xi-1)} \quad \text{(A.1)}$$

$$h_1(\beta,\xi) = \int_1^\beta \tau\,g(\beta,\xi,\tau)\,\mathrm{d}\tau = \sqrt{(\beta^2-\xi^2)(\beta^2-1)} - \frac{1}{2}(\xi^2-1)\left[\mathrm{Arccosh}\,\frac{\beta^2+\xi}{\beta(\xi+1)} + \mathrm{Arccosh}\,\frac{\beta^2-\xi}{\beta(\xi-1)}\right]$$

(A.2)

Through integration by parts and suitable analytical manipulations, it is possible to achieve the following recursive formula providing the generic function h_i as a function of h_{i-2} ($i \geq 2$):

$$h_i(\beta,\xi) = \int_1^\beta \tau^i \, g(\beta,\xi,\tau)\, d\tau = \frac{1}{i+1}\left\{(i-1)\,\xi^2\,h_{i-2}(\beta,\xi) - (\xi^2-1)\left[\text{Arccosh}\frac{\beta^2+\xi}{\beta(\xi+1)} + \text{Arccosh}\frac{\beta^2-\xi}{\beta(\xi-1)}\right] + \right.$$

$$\left. + 2i\int_1^\beta \tau^i \sqrt{\frac{\beta^2-\xi^2}{\beta^2-\tau^2}}\, d\tau - 2(i-1)\xi^2\int_1^\beta \tau^{i-2}\sqrt{\frac{\beta^2-\xi^2}{\beta^2-\tau^2}}\, d\tau\right\}$$

(A.3)

where the integrals at the right hand side can be found in closed form in classical Table of Integrals handbooks.

Figure and table captions

Figure 1. Crack Opening Displacement for a crack of length $2a$ in an infinite slab subjected to: a remote uni-axial stress σ_∞ orthogonal to the crack (a); a pair of forces P acting on the crack faces (b).

Figure 2. Cohesive crack model for a crack of length $2a$ in an infinite slab subjected to a remote uni-axial stress σ_∞: details of the process zone and of the cohesive stresses (a); generic cohesive law (b).

Figure 3. Normalized cohesive stresses and opening displacement within the process zone for $\alpha = 1$ and linear softening; real crack tip on the left ($\xi = 1$) and fictitious crack tip on the right ($\xi = \beta$): (a) $\beta = 1.691$, corresponding to the maximum remote stress ($\sigma_f = 0.478\ \sigma_c$); (b) $\beta = 1.899$, corresponding to real crack growth onset.

Figure 4. Cohesive laws with power law softening for: constant tensile strength and constant critical displacement (a); constant tensile strength and constant fracture energy (b). Cohesive laws are plotted for the following power law exponent values: $n = 0, 0.5, 1, 2, 4$.

Figure 5. Failure stress vs. crack length (a) and process zone size (at $\sigma_\infty = \sigma_f$) vs. crack length (b) for cohesive laws with different power law exponent ($n = 0, 0.5, 1, 2, 4$).

Figure 6. Stress weight functions (a); failure stress vs. crack length (b); finite crack advancement vs. crack length (c); failure stress vs. crack length, bi-logarithmic plot (d). Plots in (b,c,d) refer to weight functions in (a) having the same dashing: $\rho(t) = 3(1-t)^2$, dotted line; $\rho(t) = 1$, continuous line; $\rho(t) = 6t(1-t)$, short-dashed line; $\rho(t) = 3t^2$, dot-dashed line; $\rho(t) = \delta(1-t)$, long-dashed line.

Figure 7. Failure stress vs. crack length (a) according to FFM with different p values ($p = 0.01$, 0.3, 1, 4, 12); finite crack advancement vs. crack length (b); length where stress exceeds σ_c vs. crack length (c). Curves with the same dashing refer to the same p value.

Figure 8. Stress weight functions (a); failure stress vs. crack length according to FFM (continuous lines) and CCM (dotted lines) (b); finite crack advancement vs. crack length (c). Curves correspond to the following values: $n = 0$, 0.5, 1, 2, 4.

Figure 9. Failure stress vs. crack length (a) according to FFM − continuous lines − and to CCM − dotted lines; finite crack advancement vs. crack length (b). FFM and CCM plots correspond respectively to the following values: $p = 1.5$, 4, 6, 9, 11 and $n = 0$, 0.5, 1, 2, 4.

Figure 10. Correspondence between the power law exponent n of the cohesive law and the parameter p defining the position of the (Dirac delta) weight function.

Figure 11. Dimensionless nominal stress at failure vs. relative crack depth for TPB cracked beams for $h/l_{ch} = 4.14$ (a): LEFM (magenta line); FFM1, with uniform weight function (green line); FFM2, with Dirac weight function having $p = 6$ (blue line); CCM, with linear softening (black dots − from Carpinteri & Colombo, 1989). Nominal stress at failure vs. size, dimensionless plot (b): average stress criterion (red line); FFM1, with uniform weight function (green line); FFM2, with Dirac weight function having $p = 6$ (blue line); FFM3, with Dirac weight function having $p = 3$ (light blue line); CCM, with linear softening (black dots − from Carpinteri & Colombo, 1989).

Table 1. Correspondence between CCM cohesive laws of power law type (column 3) and FFM weight functions defined on the interval $0 < x < \Delta$ (column 2) or defined as Dirac delta functions at different locations (column 4).

References

Alfano G. (2006) On the influence of the shape of the interface law on the application of cohesive-zone models. Composites Science and Technology 66:723-730.

Barenblatt G. I (1959) The Formation of Equilibrium Cracks During Brittle Fracture: General Ideas and Hypotheses. Journal of Applied Mathematics and Mechanics 23:622-636.

Bažant Z. P. (2001) Scaling of Structural Strength. CRC Press.

Broberg K. B. (1999) Cracks and fracture. Academic Press, London.

Carpinteri A. (1989) Cusp catastrophe interpretation of fracture instability. Journal of the Mechanics and Physics of Solids 37:567-582.

Carpinteri A., Colombo G. (1989) Numerical analysis of catastrophic softening behaviour (snap-back instability). Computers & Structures. 31(4):607-636.

Carpinteri A., Cornetti P., Puzzi S. (2006) Scaling laws and multiscale approach in the mechanics of heterogeneous and disordered materials. Applied Mechanics Reviews 59:283-304.

Cornetti P., Corrado M, De Lorenzis L., Carpinteri A. (2015) An analytical cohesive crack modeling approach to the edge debonding failure of FRP-plated beams. International Journal of Solids and Structures 53:92-106.

Cornetti P., Mantič V., Carpinteri A. (2012) Finite fracture mechanics at elastic interfaces. International Journal of Solids and Structures 49:1022-1032.

Cornetti P., Pugno N., Carpinteri A., Taylor D. (2006). Finite fracture mechanics: a coupled stress and energy failure criterion. Engineering Fracture Mechanics 73:2021-2033.

Cornetti P., Sapora A., Carpinteri A. (2016) Short cracks and V-notches: Finite Fracture Mechanics vs. Cohesive Crack Model. Engineering Fracture Mechanics 168:2-12.

Dimitri R., Cornetti P., Mantič V., Trullo M., De Lorenzis L. (2017) Mode-I debonding of a double cantilever beam: A comparison between cohesive crack modeling and Finite Fracture Mechanics. International Journal of Solids and Structures 124:57-72.

Dugdale D.S. (1960) Yielding of steel sheets containing slits. Journal of the Mechanics and Physics of Solids 8:100-108.

García I.G., Paggi M., Mantič V. (2014) Fiber-size effects on the onset of fiber−matrix debonding under transverse tension: A comparison between cohesive zone and finite fracture mechanics models. Engineering Fracture Mechanics 115:96–110.

Hashin Z. (1996) Finite thermoelastic fracture criterion with application to laminate cracking analysis. Journal of the Mechanics and Physics of Solids 44:1129-1145.

Hebel J., Dieringer R., Becker, W. (2010) Modelling brittle crack formation at geometrical and material discontinuities using a finite fracture mechanics approach. Engineering Fracture Mechanics, 77:3558-3572.

Henninger C., Leguillon D., Martin E. (2007) Crack initiation at a V-notch − comparison between a brittle fracture criterion and the Dugdale cohesive model. Comptes Rendu Mécanique 335:388-393.

Hillerborg A., Modeer M., Petersson P. E. (1976) Analysis of Crack Formation and Crack Growth in Concrete by Means of Fracture Mechanics and Finite Elements. Cement and Concrete Research 6:773–782.

Karihaloo B.L., Xiao Q.Z. (2001) Higher order terms of the crack tip asymptotic field for a notched three-point bend beam. International Journal of Fracture. 112:111–128.

Leguillon D. (2002) Strength or toughness? A criterion for crack onset at a notch. European Journal of Mechanics A/Solids 21:61-72.

Lenci S. (2001) Analysis of a crack at a weak interface. International Journal of Fracture 108:275-290.

Martin E., Vandellos T., Leguillon D., Carrère N. (2016) Initiation of edge debonding: coupled criterion versus cohesive zone model. International Journal of Fracture 199:157-168.

Murer S., Leguillon D. (2010) Static and fatigue failure of quasi-brittle materials at a V-notch using a Dugdale model. European Journal of Mechanics A/Solids 29, 109-118.

Needleman A. (1990) An analysis of decohesion along an imperfect interface. International Journal of Fracture 42:21-40.

Rosendahl P.L., Weißgraeber P., Stein N., Becker W. (2017) Asymmetric crack onset at open-holes under tensile and in-plane bending loading. International Journal of Solids and Structures 113-114:10-23.

Shet C., Chandra N. (2004) Effect of the Shape of T–δ Cohesive Zone Curves on the Fracture Response. Mechanics of Advanced Materials and Structures 11, 249-275.

Stein N., Weißgraeber P., Becker W. (2015) A model for brittle failure in adhesive lap joints of arbitrary joint configuration. Composite Structures 133:707-718.

Sun Z., Ooi E.T., Song C. (2015) Finite fracture mechanics analysis using the scaled boundary finite element method. Engineering Fracture Mechanics, 134:330-353.

Tada H., Paris P.C., Irwin G.R. (2000) The stress analysis of cracks handbook – 3rd edition. ASME Press, New York.

Távara L., García I.G., Vodička R., Panagiotopoulos C.G., Mantič V. (2016) Revisiting the problem of debond initiation at fibre-matrix interface under transversal biaxial loads. A comparison of several non-classical fracture mechanics approaches. Key Engineering Materials 713:232-235.

Taylor D. (2007) The Theory of Critical Distances. Elsevier, Oxford.

Xu W., Thorsson S. I., Waas A. M. (2015) Experimental and numerical study on cross-ply woven textile composite with notches and cracks. Composite Structures 132:816–824.

Xu W., Waas A. M. (2017) Multiple solutions in cohesive zone models of fracture. Engineering Fracture Mechanics 177:104–122.

Xu W., Wang H., Wu X., Zhang X., Bai G., Huang X. (2014) A novel method for residual strength prediction for sheets with multiple site damage: Methodology and experimental validation. International Journal of Solids and Structures 51:551-565.

Wang J.T. (2013) Investigating Some Technical Issues on Cohesive Zone Modeling of Fracture. Journal of Engineering Materials and Technology-Transactions of the ASME 135, Art. No. 011003.

Table 1

n	Weight function 1 $\rho(x/\Delta), 0 < x < \Delta$	Power cohesive law $\sigma_{coh}(w), 0 < w < w_c$	Weight function 2 $\rho(x/\Delta)$	p
n	$n\left(1 - x/\Delta\right)^{n-1}$	$\sigma_c\left(1 - w/w_c\right)^n$	$\delta(1 - p\,x/\Delta)$	p
0	$\delta(1 - x/\Delta)$	σ_c	$\delta(1 - 3x/2\Delta)$	1.5
0.5	$\left(2\sqrt{1 - x/\Delta}\right)^{-1}$	$\sigma_c\sqrt{1 - w/w_c}$	$\delta(1 - 4\,x/\Delta)$	4
1	1	$\sigma_c\left(1 - w/w_c\right)$	$\delta(1 - 6\,x/\Delta)$	6
2	$2\left(1 - x/\Delta\right)$	$\sigma_c\left(1 - w/w_c\right)^2$	$\delta(1 - 9\,x/\Delta)$	9
4	$4\left(1 - x/\Delta\right)^3$	$\sigma_c\left(1 - w/w_c\right)^4$	$\delta(1 - 11\,x/\Delta)$	11

Table 1. Correspondence between CCM cohesive laws of power law type (column 3) and FFM weight functions defined on the interval $0 < x < \Delta$ (column 2) or defined as Dirac delta functions at different locations (column 4).

Figure 1
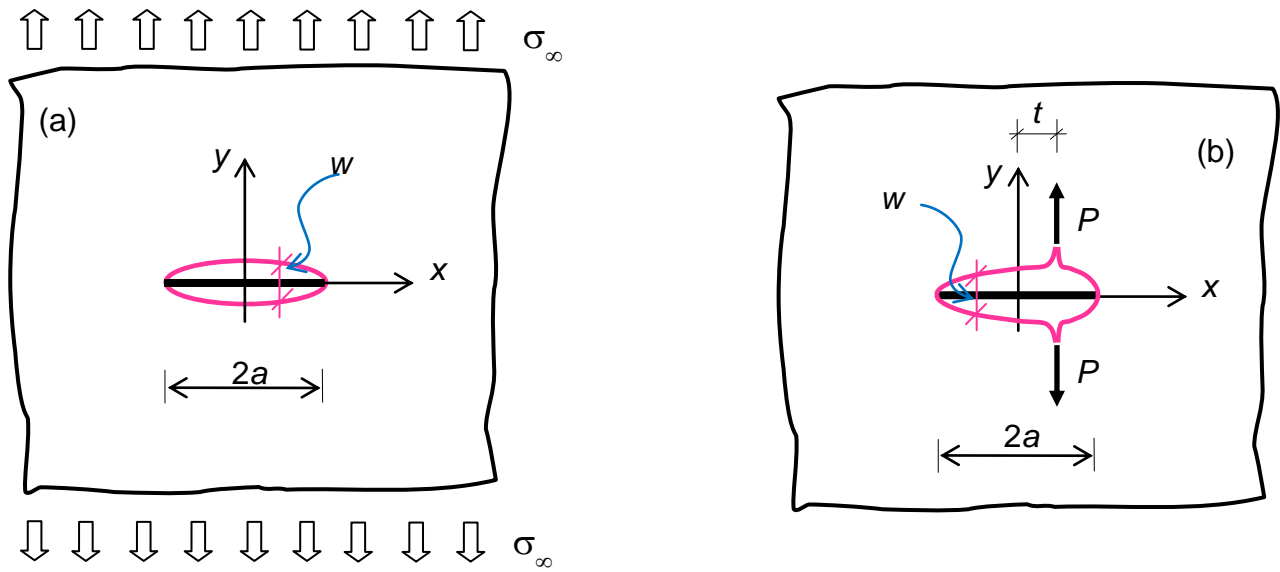
Figure 1. Crack Opening Displacement for a crack of length $2a$ in an infinite slab subjected to: a remote uni-axial stress σ_∞ orthogonal to the crack (a); a pair of forces P acting on the crack faces (b).
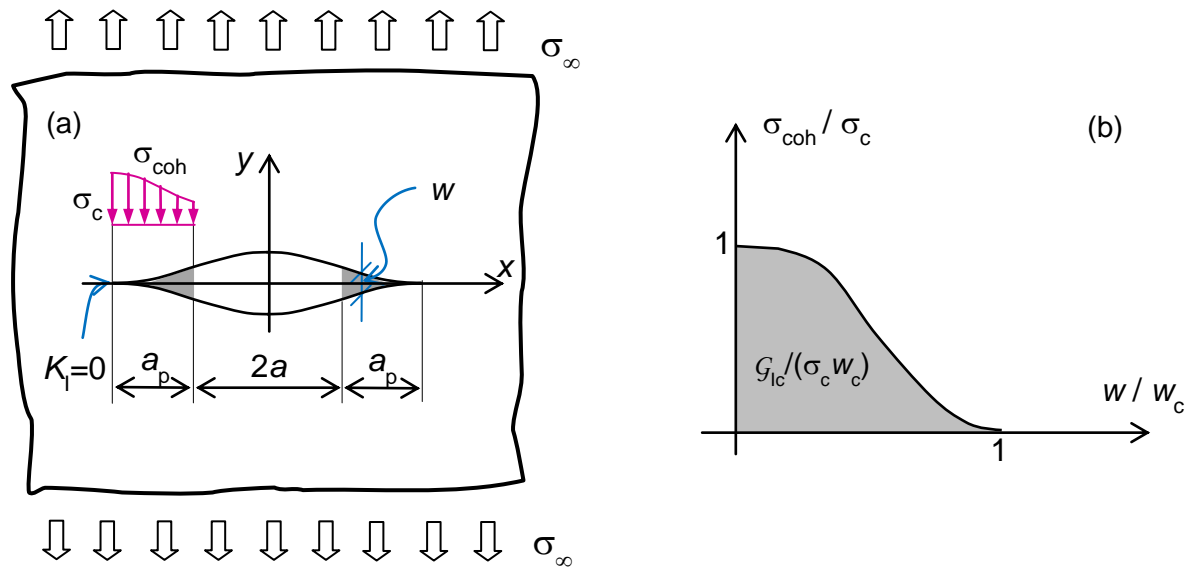
Figure 2

Figure 2. Cohesive crack model for a crack of length $2a$ in an infinite slab subjected to a remote uni-axial stress σ_∞: details of the process zone and of the cohesive stresses (a); generic cohesive law (b).
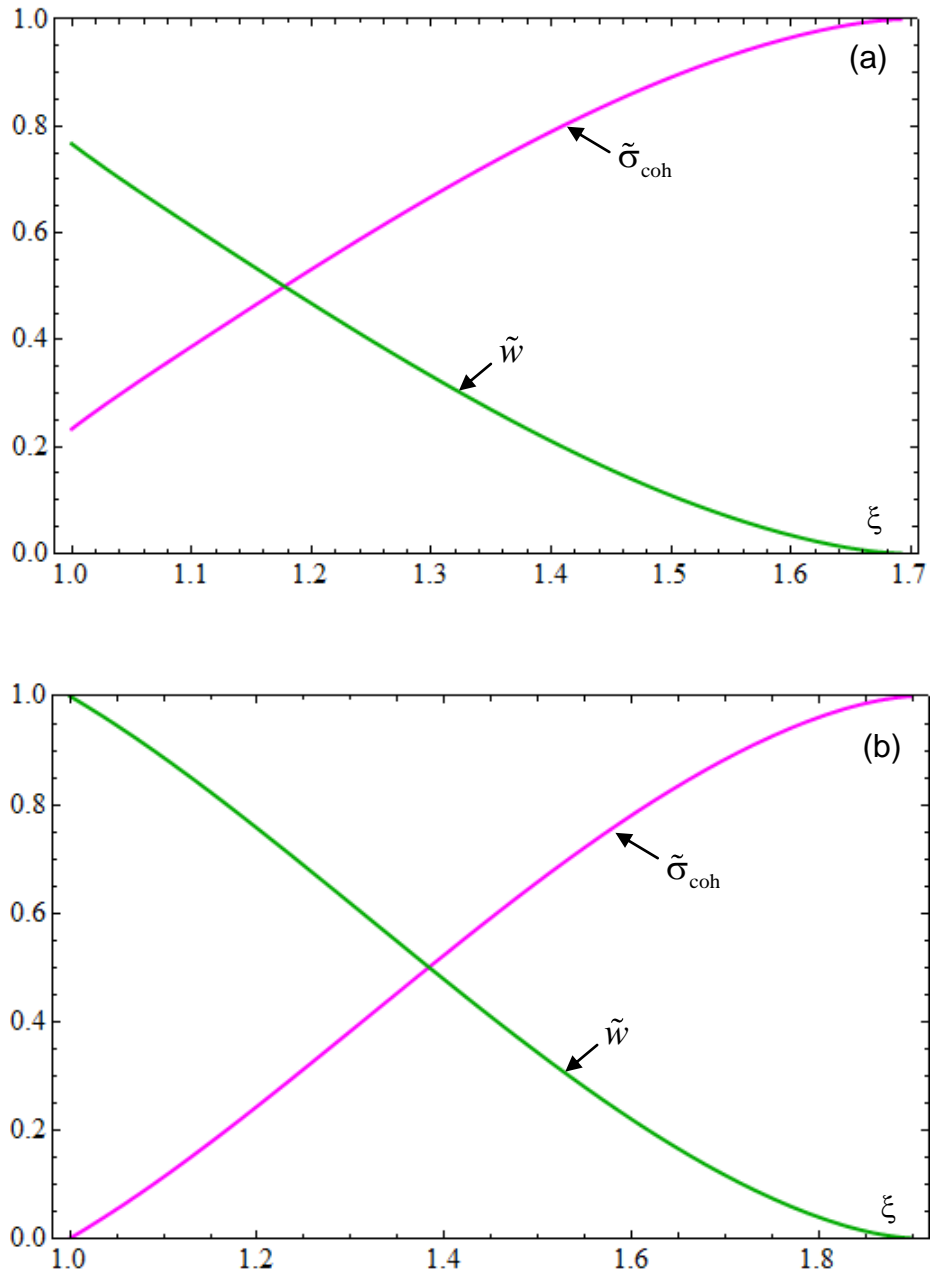
Figure 3

Figure 3. Normalized cohesive stresses and opening displacement within the process zone for $\alpha = 1$ and linear softening; real crack tip on the left ($\xi = 1$) and fictitious crack tip on the right ($\xi = \beta$): (a) $\beta = 1.691$, corresponding to the maximum remote stress ($\sigma_f = 0.478\ \sigma_c$); (b) $\beta = 1.899$, corresponding to real crack growth onset.
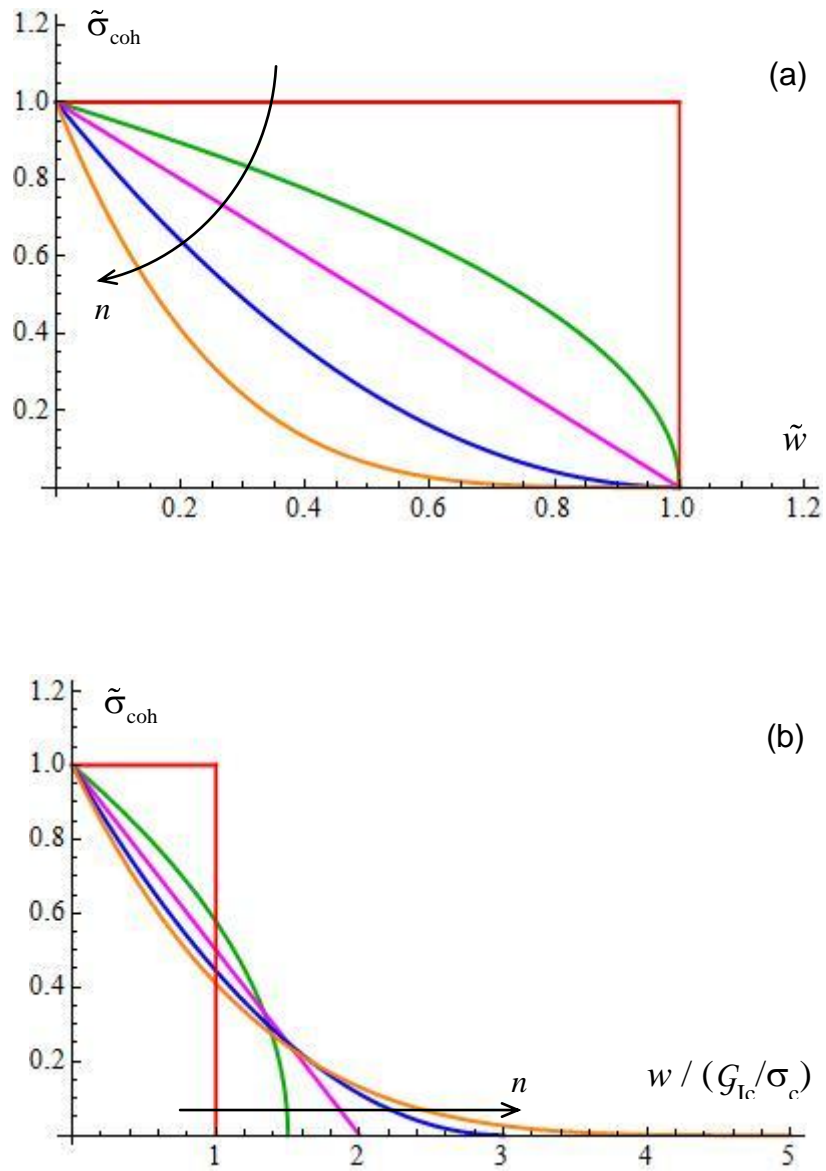
Figure 4

Figure 4. Cohesive laws with power law softening for: constant tensile strength and constant critical displacement (a); for constant tensile strength and constant fracture energy (b). Cohesive laws are plotted for the following power law exponent values: $n = 0, 0.5, 1, 2, 4$.
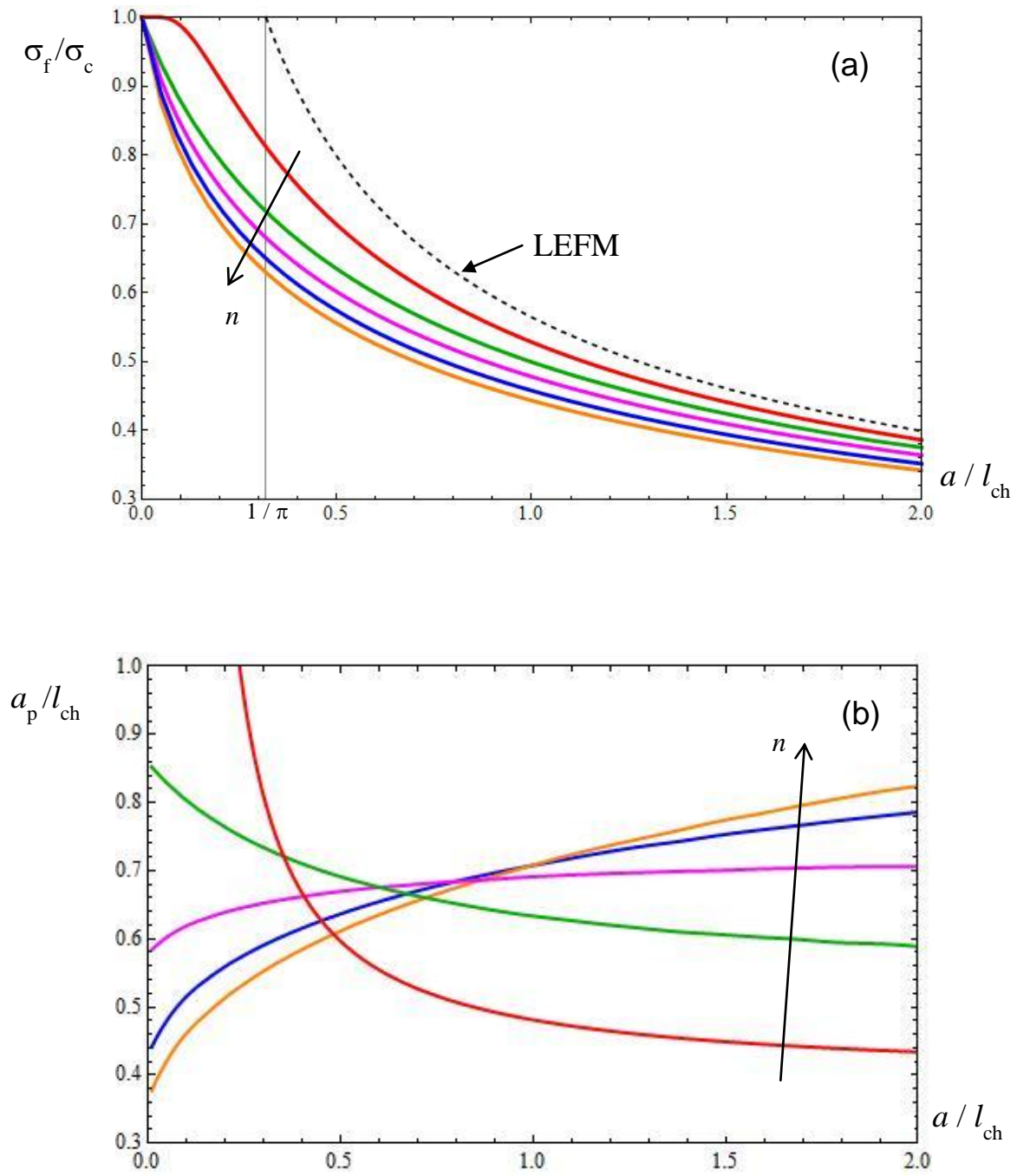
Figure 5

Figure 5. Failure stress vs. crack length (a) and process zone size (at $\sigma_\infty = \sigma_f$) vs. crack length (b) for cohesive laws with different power law exponent ($n = 0, 0.5, 1, 2, 4$).
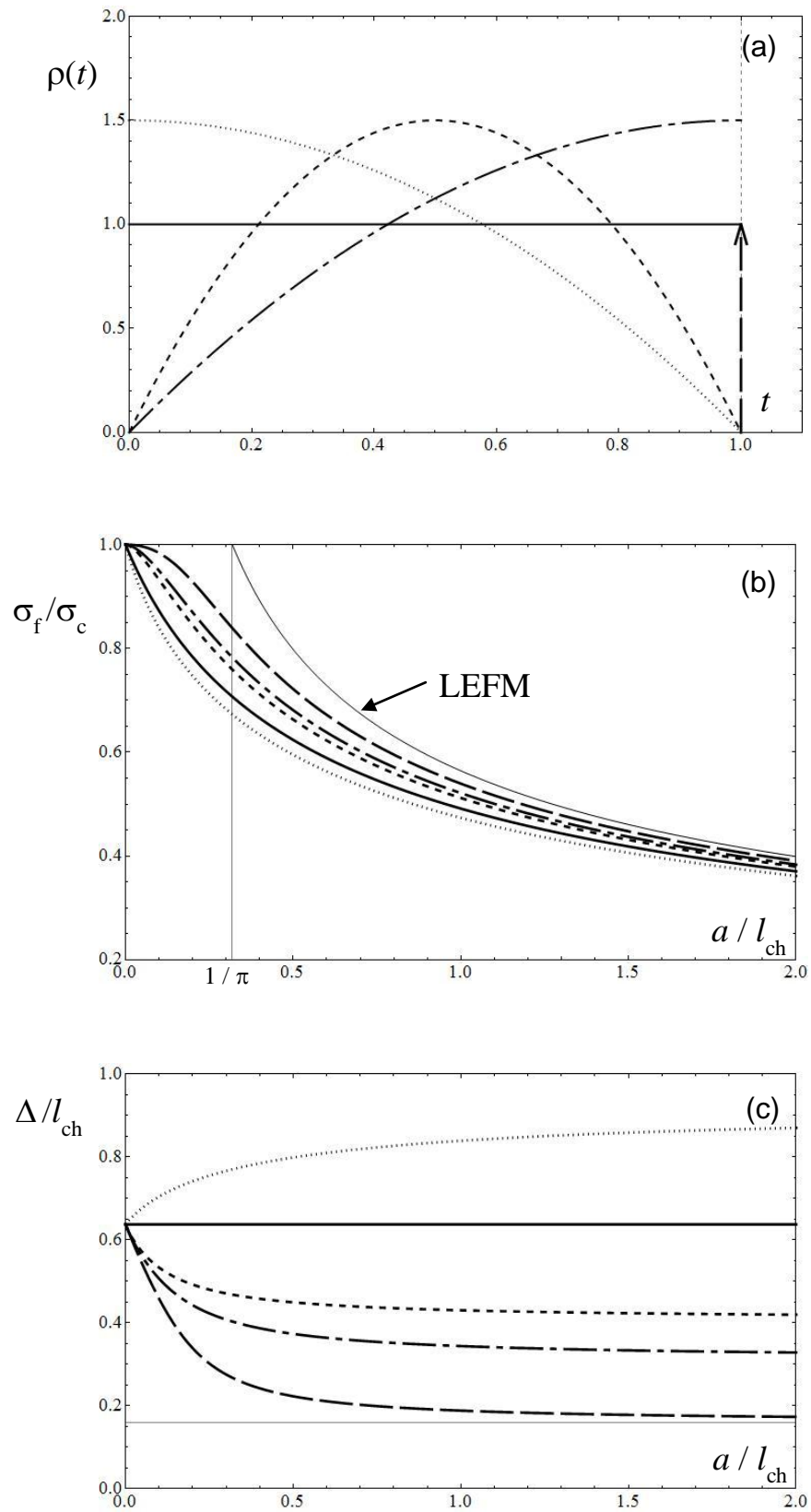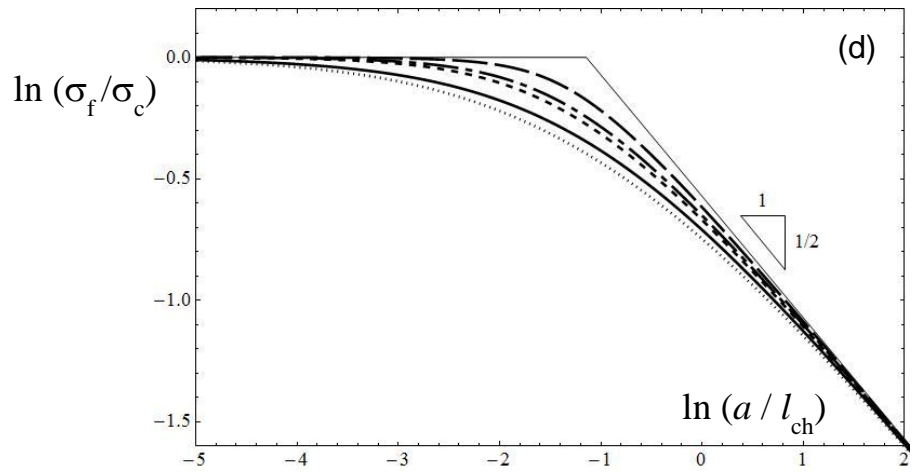
Figure 6

Figure 6. Stress weight functions (a); failure stress vs. crack length (b); finite crack advancement vs. crack length (c); failure stress vs. crack length, bi-logarithmic plot (d). Plots in (b,c,d) refer to weight functions in (a) having the same dashing: $\rho(t) = 3(1-t)^2$, dotted line; $\rho(t) = 1$, continuous line; $\rho(t) = 6t(1-t)$, short-dashed line; $\rho(t) = 3t^2$, dot-dashed line; $\rho(t) = \delta(1-t)$, long-dashed line.
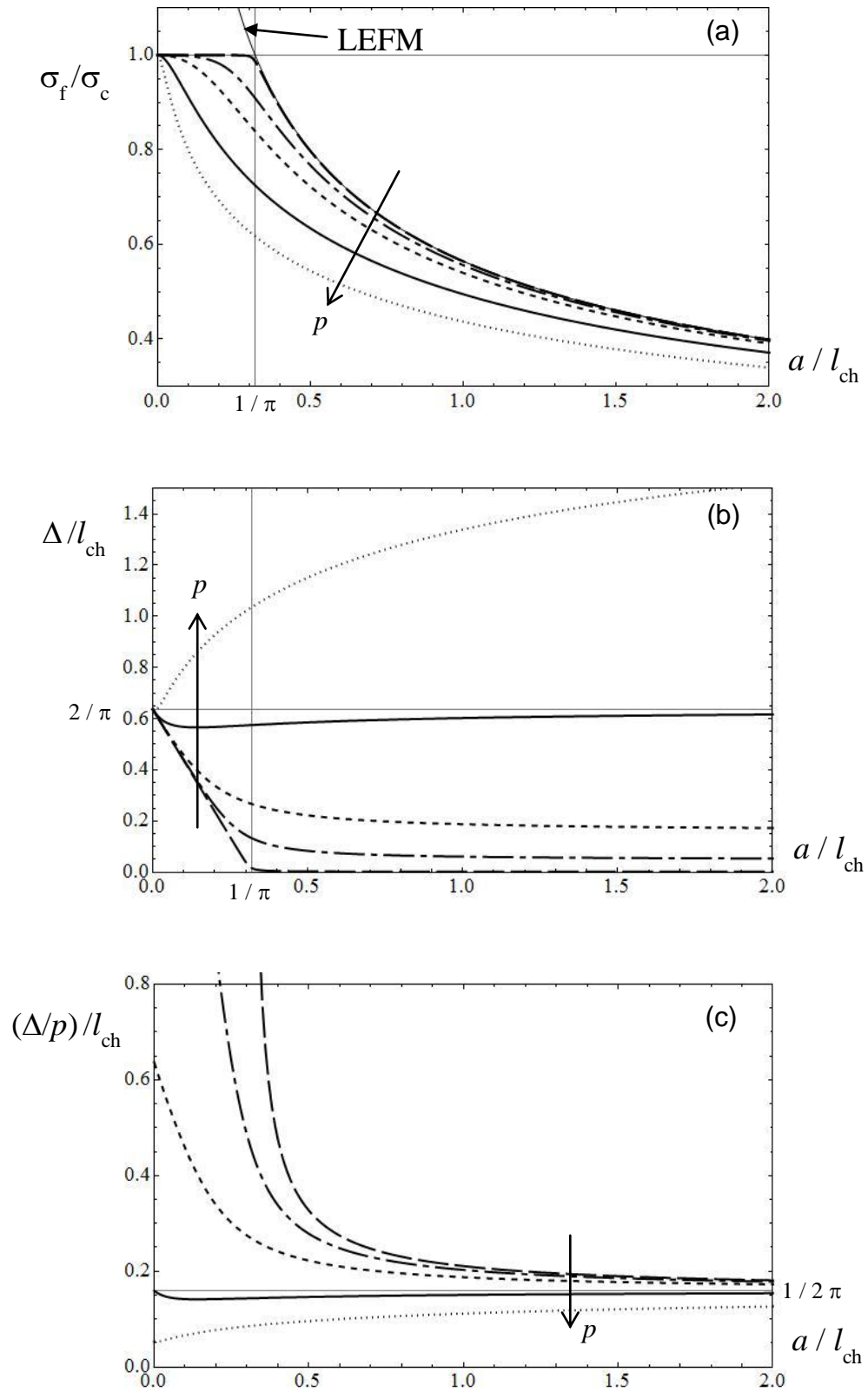
Figure 7

Figure 7. Failure stress vs. crack length (a) according to FFM with different p values ($p = 0.01$, 0.3, 1, 4, 12); finite crack advancement vs. crack length (b); length where stress exceeds σ_c vs. crack length (c); dimensionless plots. Curves with the same dashing refer to the same p value.
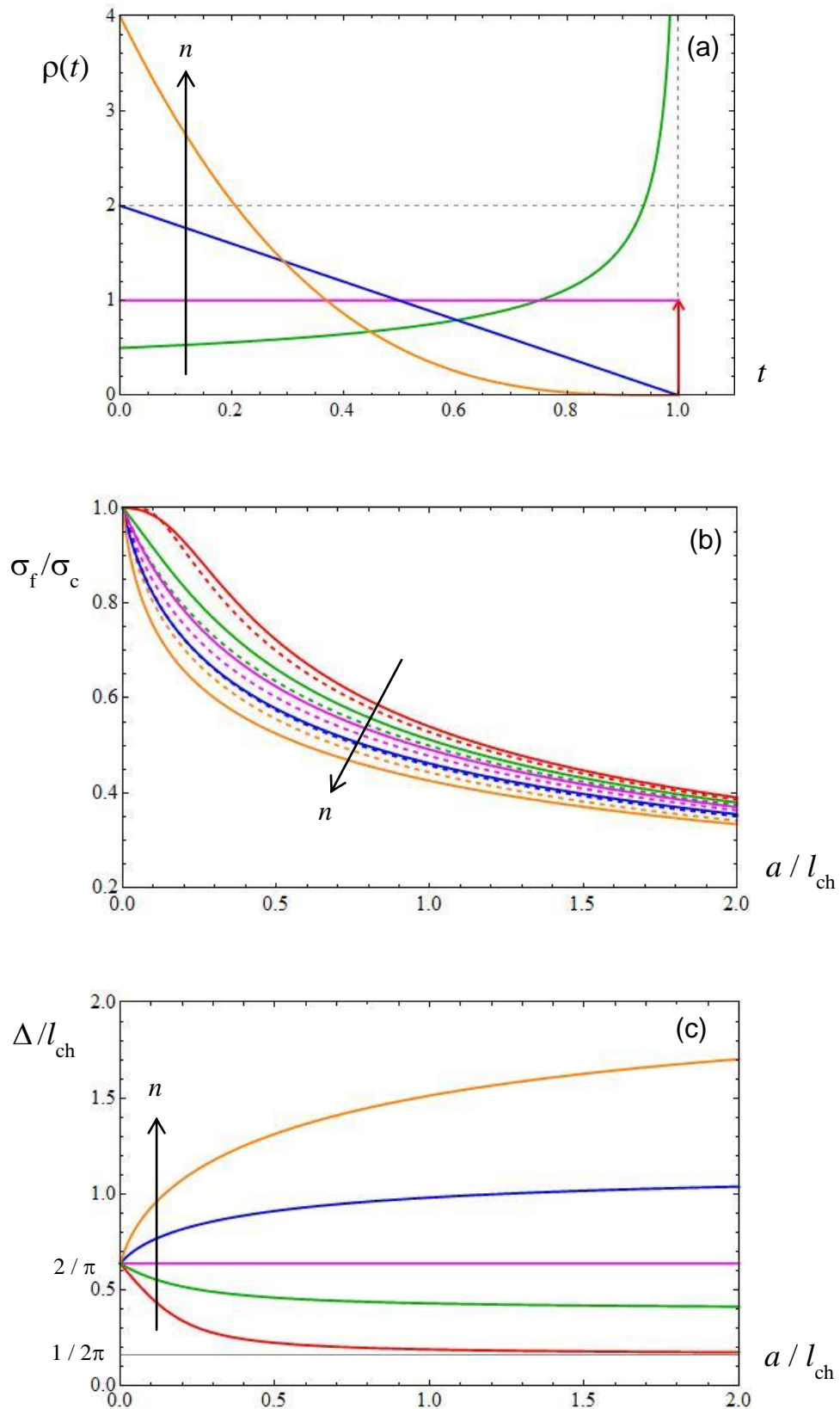
Figure 8

Figure 8. Stress weight functions (a); failure stress vs. crack length according to FFM (continuous lines) and CCM (dotted lines) (b); finite crack advancement vs. crack length (c). Curves correspond to the following values: $n = 0, 0.5, 1, 2, 4$.
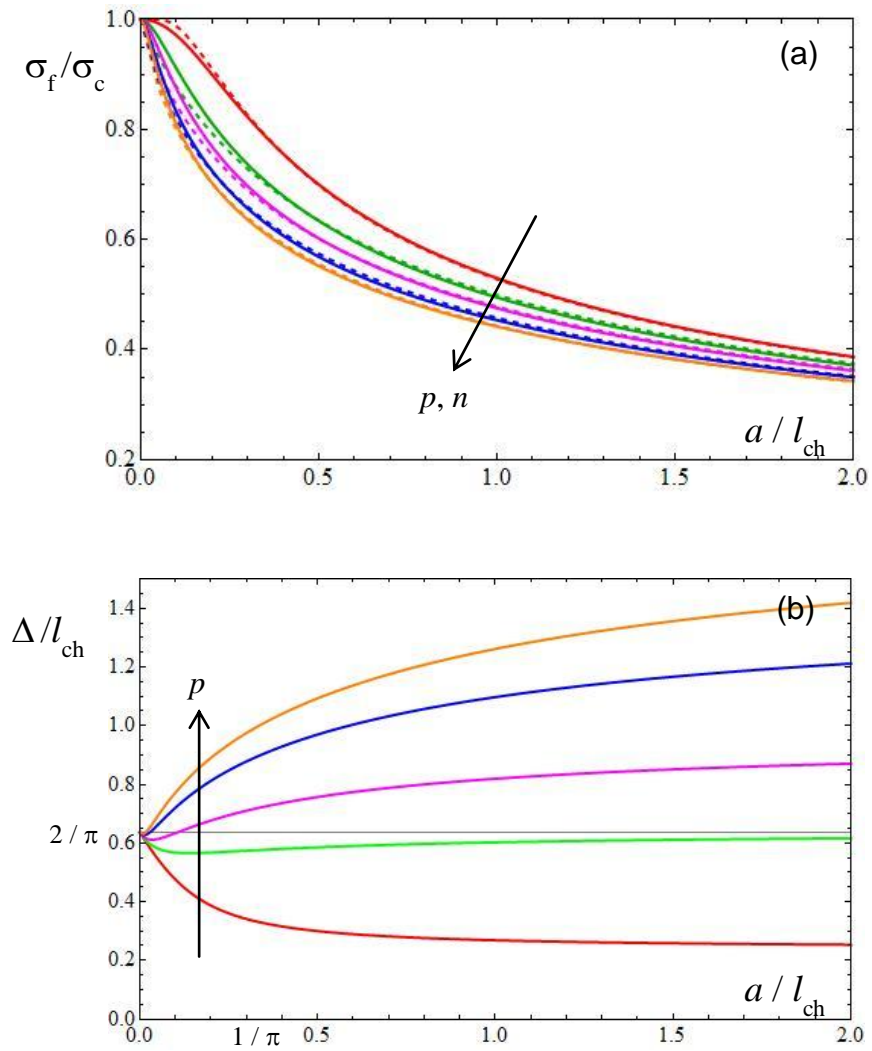
Figure 9

Figure 9. Failure stress vs. crack length (a) according to FFM − continuous lines − and to CCM − dotted lines; finite crack advancement vs. crack length (b). FFM and CCM plots correspond respectively to the following values: $p = 1.5, 4, 6, 9, 11$ and $n = 0, 0.5, 1, 2, 4$.
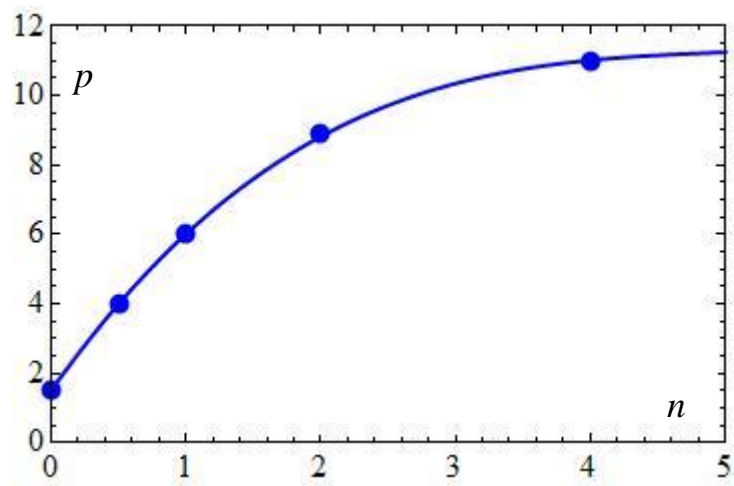
Figure 10

Figure 10. Correspondence between the power law exponent *n* of the cohesive law and the parameter *p* defining the position of the (Dirac) weight function.
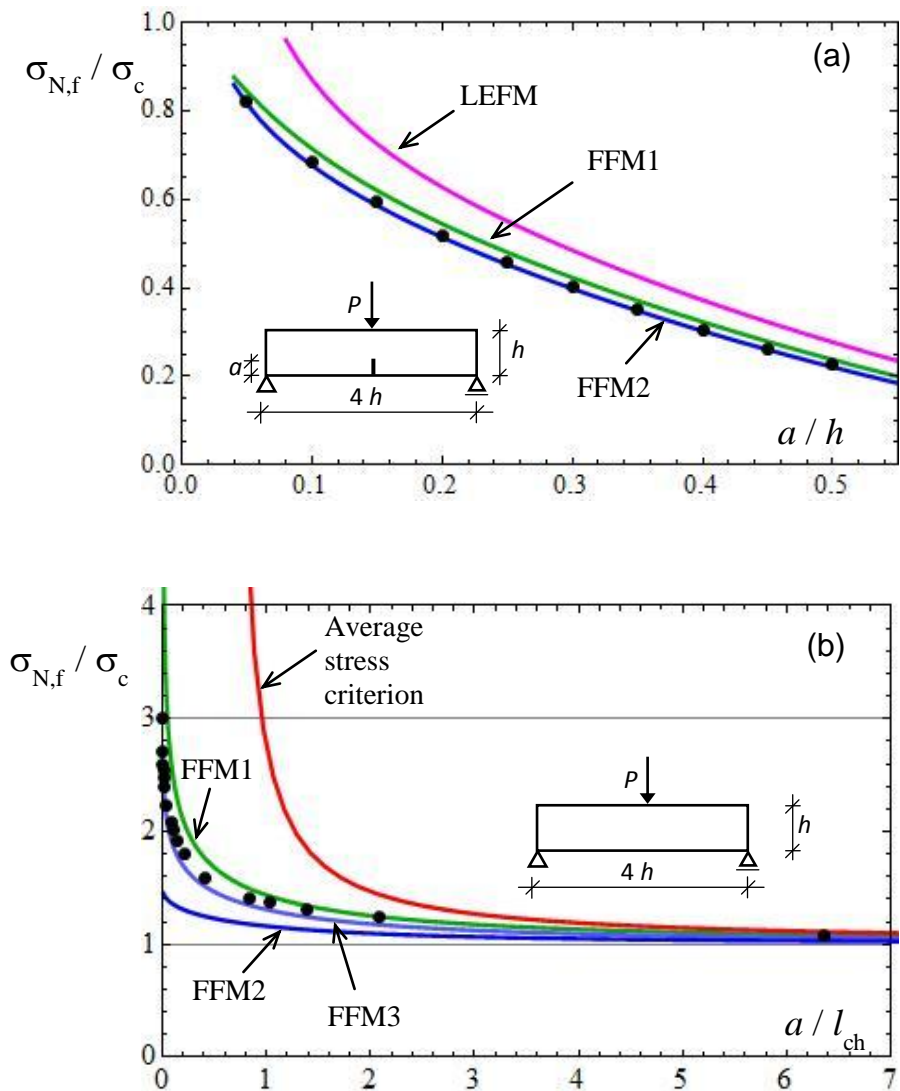
Figure 11

Figure 11. Dimensionless nominal stress ($6P/h$) at failure vs. relative crack depth for TPB cracked beams for $h/l_{ch} = 4.14$ (a): LEFM (magenta line); FFM1, with uniform weight function (green line); FFM2, with Dirac weight function having $p = 6$ (blue line); CCM, with linear softening (black dots − from Carpinteri & Colombo, 1989). Nominal stress at failure vs. size, dimensionless plot (b): average stress criterion (red line); FFM1, with uniform weight function (green line); FFM2, with Dirac weight function having $p = 6$ (blue line); FFM3, with Dirac weight function having $p = 3$ (light blue line); CCM, with linear softening (black dots − from Carpinteri & Colombo, 1989).